Spine Deformity

www.spine-deformity.org

Spine Deformity 1 (2013) 2–9

Contributions of Remodeling and Asymmetrical Growth to Vertebral Wedging in a Scoliosis Model

David D. Aronsson, MD*, Ian A.F. Stokes, PhD, Carole A. McBride, BS

Department of Orthopaedics and Rehabilitation, University of Vermont, Robert T. Stafford Hall, 95 Carrigan Drive Burlington, VT, 05405, USA

Received 6 March 2012; revised 1 July 2012; accepted 31 July 2012

Abstract

Study Design: We performed a laboratory study of rats of 3 different ages with imposed angulation and compressive loading to caudal vertebrae to determine causes of vertebral wedging.

Objectives: The purpose was to determine the percentage of total vertebral wedging that was caused by asymmetric growth, vertebral body, and epiphyseal wedging. Approval from the Institutional Animal Care and Use Committee, the University of Vermont, was obtained for the live animal procedures used in this study.

Background Summary: Vertebral wedging from asymmetrical growth (Hueter-Volkmann law) is reported to cause vertebral wedging in scoliosis with little attention to the possible contribution of bony remodeling (Wolff's law).

Methods: In our study, an external fixator imposed a 30° lateral curvature and compression of 0.1 megapascal (MPa) in 5- and 14-week-old animals (Groups 1 and 2) and 0.2 MPa in 14- and 32-week-old animals (groups 3 and 4). Total vertebral wedging was measured from micro CT scans. Wedging due to asymmetrical growth and epiphyseal remodeling was calculated from fluorescent labels and the difference was attributed to vertebral body wedging.

Results: Total vertebral wedging averaged 18°, 6°, 10° and 5° in Groups 1, 2, 3, and 4, respectively. Metaphyseal asymmetrical growth averaged 8°, 1°, 4°, 0° (44%, 17%, 40% and 0% of total). Epiphyseal wedging averaged 9°, 0°, 3°, and -1°. The difference (vertebral body) averaged 1°, 5°, 3°, and 7° (6%, 83%, 30% and 140% of total). The growth of the loaded vertebrae as a percentage of control vertebrae was 56%, 39% and 25% in Groups 1, 2 and 3; negligible in Group 4. Vertebral body cortical remodeling, with increased thickness and increased curvature on the concave side was evident in young animals and 0.2 MPa loaded older animals.

Conclusions: We conclude that asymmetrical growth was the largest contributor to vertebral wedging in young animals; vertebral body remodeling was the largest contributor in older animals. If, conversely, vertebral wedging can be corrected by appropriate loading in young and old animals, it has important implications for the nonfusion treatment of scoliosis.

Keywords: Scoliosis; Vertebral wedging; Vertebral remodeling (Wolff's law); Asymmetric growth (Heuter-Volkmann law); Mechanical modulation

Introduction

The natural history of adolescent idiopathic scoliosis (AIS) consists of 3 stages: the initiation of the curve, progression associated with rapid growth during puberty, and subsequent slow progression in some patients, particularly with curves over 50°, or stabilization in other patients after skeletal maturity. The key risk factors for progression include the magnitude of the curve and the age at onset; large curves in young patients have the highest risk [1]. Although scoliosis includes both vertebral and disc wedging, the relative contributions and timing of their development are not well documented.

Basic science principles and prior studies suggest that the rapid progression of vertebral wedging in AIS during the adolescent growth spurt is caused by asymmetrical growth [2,3]. This is attributed to the Hueter-Volkmann law of mechanically modulated endochondral growth with growth retarded by compression and accelerated by reduced compression [4]. If a spine with scoliosis has greater loading on the concave side, this asymmetrical loading with compression on the concave side causes asymmetrical

Author disclosures: DDA (grant from the Scoliosis Research Society, consultancy for Canadian Institutes of Health Research) IAS (consulting to Kspine, Inc.); CAM (none).

This work is supported by a grant from the Scoliosis Research Society.

*Corresponding author. Department of Orthopaedics and Rehabilitation, Robert T. Stafford Hall, Room 434B, 95 Carrigan Drive, University of Vermont, Burlington, VT 05405-0084, USA. Tel.: (802) 656-2250; fax: (802) 656-4247.

E-mail address: david.aronsson@uvm.edu (D.D. Aronsson).

2212-134X/$ - see front matter © 2013 Scoliosis Research Society.
http://dx.doi.org/10.1016/j.jspd.2012.07.006

growth, creating vertebral wedging, and leading to the "vicious cycle" of scoliosis progression [4,5]. A goat model study created scoliosis using an asymmetric posterior tether and reported some correction of the deformity using anterior convex staples [6]. It has been hypothesized that if the load asymmetry could be reversed, the vicious cycle would be reversed, and the scoliosis curve would be corrected [7].

These basic science studies have created enthusiasm to use growth modulation in skeletally immature patients with early onset scoliosis to correct the scoliosis rather than performing an early in situ fusion. A clinical study in young patients with AIS treated by convex stapling reported that none of the patients with preoperative curves less than 30° progressed, whereas 18% of preoperative curves greater than or equal to 30° progressed [8].

Although progression of AIS during the adolescent growth spurt is thought to be secondary to asymmetrical growth, vertebral body remodeling may also contribute to the vertebral wedging according to the principles of Wolff's law [2]. This law states that bone tissue remodels over time in response to prevailing mechanical demands [9], with internal remodeling [10,11] as well as possibly alteration of external shape [12].

Long bone fractures in children are known to remodel and correct angular deformity spontaneously. The remodeling is thought to occur by asymmetrical growth, but fracture angulation may also correct by diaphyseal remodeling [12].

A literature search did not locate any study that evaluated the role of remodeling of the vertebral body in the development of vertebral wedging in scoliosis, which is the topic of the present study. The purpose of this study was to test the hypothesis that vertebral wedging is caused by a combination of asymmetrical growth, vertebral body remodeling, and epiphyseal remodeling (Fig. 1). We also tested the hypothesis that the major contribution to vertebral wedging is asymmetrical growth in young animals and vertebral body remodeling in older animals. If vertebral wedging is caused by both mechanisms, it may have important implications for the treatment of AIS particularly in older patients.

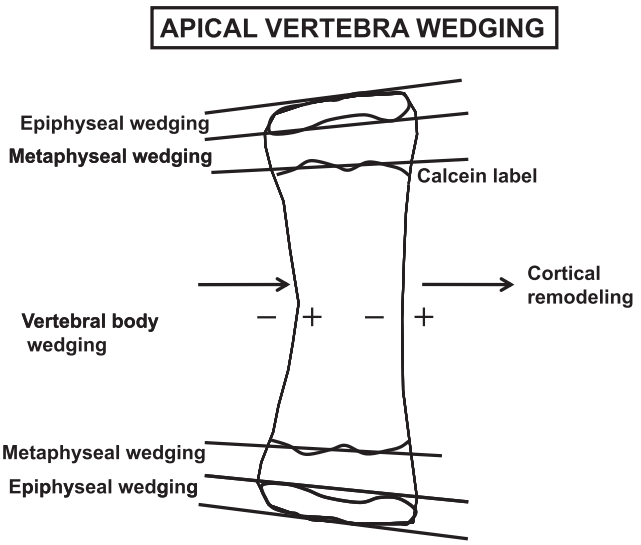

Fig. 1. Drawing showing the methods used to measure the different components of the total vertebral wedging. The total vertebral wedging was the angle between lines drawn along the vertebral endplates. The epiphyseal wedging was the sum of the angles between a line drawn along the vertebral endplate and a line drawn along the growth plate at each end of the vertebra. The metaphyseal wedging (asymmetrical growth) was the sum of the angles between a line drawn along the growth plate and a line drawn along the calcein label in the metaphysis at each end of the vertebra, then adjusted for the time from labeling to euthanasia relative to the duration of the experiment. The vertebral body remodeling was calculated (inferred) by subtracting the epiphyseal and metaphyseal wedging from the total vertebral wedging. Two hypothetical mechanisms may explain how the asymmetrical vertebral body remodeling may have developed. First, a shortening of the cortex on the concave side and a lengthening of the cortex on the convex side, resulting in bending of the vertebra; or second, a preferential concave side resorption (−) and convex side apposition (+) of bone at internal and external surfaces of the cortex producing apparent vertebral body drift or translation toward the convex side of the imposed curve.

Materials and Methods

Forty Sprague-Dawley rats were studied for 6 weeks after installation of an Ilizarov-type external fixator attached to the eighth and tenth caudal vertebrae by transfixing 0.35 mm diameter stainless-steel pins that were percutaneously placed under general anesthesia (ketamine 40 mg/kg to 80 mg/kg and xylazine 5 mg/kg to 10 mg/kg) with fluoroscopic guidance (Fig. 2A). The method was an adaptation of the method described by MacLean et al. [13]. A 30° lateral curvature was created between the eighth and tenth caudal vertebrae by the fixator. The ninth vertebra was the experimental vertebra and the seventh was the within-animal control vertebra (Fig. 2B). These parameters were selected because in prior studies incorporating 1 vertebra and 2 discs with an imposed 30° lateral curvature, the wedging initially was entirely in the intervertebral discs, but by 6 weeks the wedging of the discs and vertebrae were approximately equal [2,14].

The animals were divided into 4 groups with 10 animals in each group: group 1, 5-week old immature animals with 30° lateral curvature and 0.1 megapascal (MPa) compression; group 2, 14-week old mature animals with 30° lateral curvature and 0.1 MPa compression; group 3, 14-week old mature animals with 30° lateral curvature and 0.2 MPa compression; and group 4, 32-week old adult animals with 30° lateral curvature and 0.2 MPa compression. The animals included 5-week old animals growing at a fast rate (adolescent growth spurt), 14-week old animals growing at a slower rate (past peak growth velocity), and 32-week old animals not growing (Risser 5).

Operative technique

The animals were acclimated to the animal-care facility for 6 days before the operation. Sulfatrim (Actavis US, Morristown, New Jersey) was placed in the drinking water (intended dose 30 mg/kg to 50 mg/kg) as a prophylactic

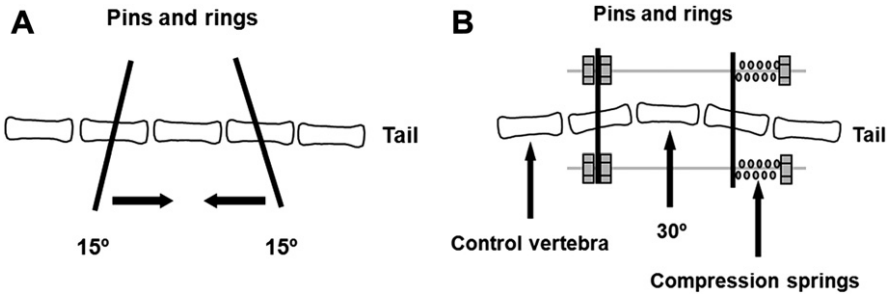

Fig. 2. Drawing showing the rat tail with the Ilizarov-type rings each placed at a 15° angle from the end plates of the vertebra. The arrows show that when the rings are brought to parallel a 30° scoliosis is created between the rings (A). Drawing showing the parallel Ilizarov-type rings creating a 30° scoliosis between the eighth and tenth vertebrae. Longitudinal rods and springs have been installed to apply asymmetrical loading of either 0.1 or 0.2 MPa (B).

antibiotic and to decrease the risk of postoperative pin tract infections. After acclimation, the animals were anesthetized and the tails were prepped with povidone-iodine scrub, followed by 70% Isopropyl Alcohol (Hydrox Laboratories, Elgin, Illinois), and Betadine solution (povidone-iodine 10%, Purdue Frederick Co, Norwalk, Connecticut). Intraoperative fluoroscopy-guided percutaneous placement of 2 0.35 mm diameter pins that were passed through perpendicular holes in carbon fiber rings, attaching them to the eighth and tenth vertebrae. The ninth vertebra was the experimental level and the seventh vertebra served as the control (Fig. 3A). The pins were placed using a hand-chuck device in the soft bone of the immature animals; an oscillating drill (Stryker, Kalamazoo, Michigan) was used in the hard bone of the mature and adult animals. During pin placement, each ring was set at a 15° angle to the tail axis (Fig. 3B). The rings were then realigned parallel by means of springs on 4 threaded rods passing through holes in the rings, imposing a 30° lateral curvature with asymmetric compression on the tail segment (Fig. 3C). The total spring force was proportional to the estimated area of the vertebra and its magnitude was set to produce 0.1 or 0.2 MPa compressive stress, using a published relationship of area to body weight [15]. Postoperatively, Buprenorphine (Hospira, Lake Forest, Illinois) 0.05 mg/kg to 0.1 mg/kg was administered subcutaneously with 3 additional doses at 12-hour intervals.

Post-surgery procedures

Spring forces were adjusted weekly to maintain constant static compression stress of 0.1 MPa (groups 1 & 2) or 0.2 MPa (groups 3 & 4). Micro computed tomography (CT) scans were performed under anesthesia postoperatively and 6 weeks later to measure wedging of experimental and control vertebrae (Figs. 4A and 4B). Calcein Green 45 mg/kg (Sigma Chemical Company, St. Louis, Missouri) was injected intraperitoneally at week 1 (week 0 for group 4) and Xylenol Orange 90 mg/kg (Sigma Chemical Company, St. Louis, Missouri) was injected subcutaneously 24 hours before euthanasia to label new bone formation (Figs. 5A through 5C).

Animals were euthanized after 6 weeks and the experimental ninth and within-animal control seventh caudal vertebrae were harvested. Each vertebra was bisected along the coronal plane and the dorsal half was fixed, dehydrated, and processed for embedding undecalcified in Epon-Araldite resin. The ventral half was fixed, decalcified, and embedded in paraffin. The Epon-Araldite resin-embedded sections were imaged using fluorescent microscopy and the

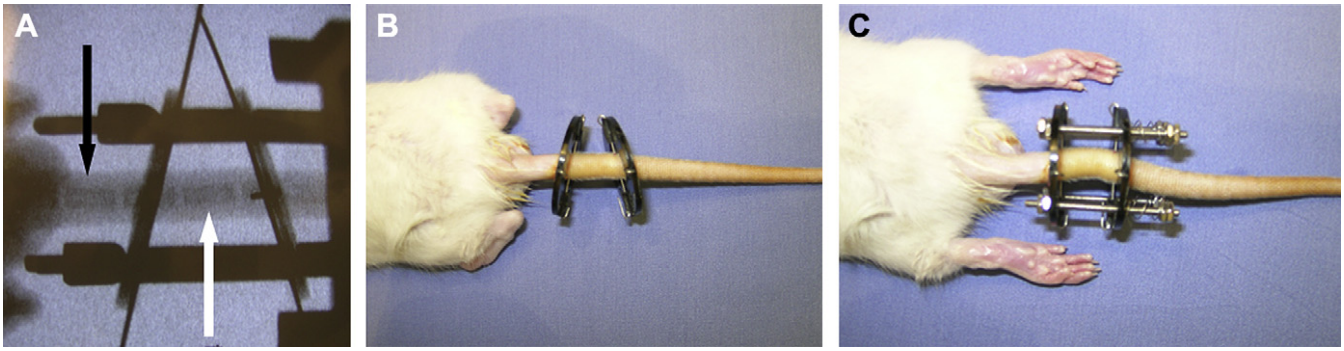

Fig. 3. Intraoperative fluoroscopic image showing the Ilizarov-type rings placed at 15° angle from the end plates of the eighth and tenth caudal vertebrae. The experimental vertebra (white arrow) and proximal control vertebra (black arrow) are shown (A). Intraoperative photograph showing the Ilizarov-type rings each placed at 15° angle from the end plates of the eighth and tenth vertebrae (B). Postoperative photograph showing Ilizarov-type rings are parallel imposing a 30° scoliosis and longitudinal rods have been installed to hold springs that apply asymmetrical loading of either 0.1 or 0.2 MPa (C).

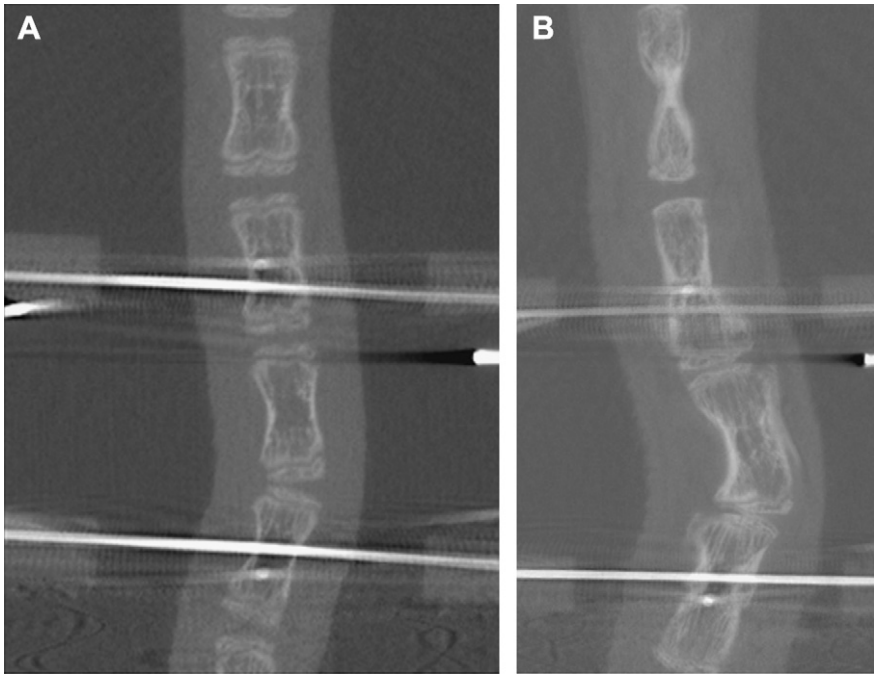

Fig. 4. Postoperative micro CT Scan showing the Ilizarov-type rings installed on the eighth and tenth caudal vertebrae with longitudinal rods connecting the rings to impose a 30° scoliosis and with springs to apply asymmetrical loading. The experimental vertebra has a bi-concave morphology (A). Micro CT Scan 6 weeks after the operation showing that the experimental vertebra has become wedged with increased concavity on the concave side and decreased concavity on the convex side. The loaded vertebra is gradually drifting or translating toward the convexity (B).

paraffin-embedded sections were stained with Hematoxylin and Eosin for light microscopy.

Measurement techniques

Microscopic and CT images were measured using specially written MatLab (The MathWorks, Natick, Massachusetts) codes to calculate wedging angles and growth. On the micro CT scan coronal plane images, 2 points were marked on each superior and inferior end plate of the experimental and control vertebrae. A line connecting these points was parallel to the respective vertebral end plates; the total vertebral wedging was the Cobb angle between these 2 lines (Fig. 1).

The vertebral body shape was calculated by computer-assisted analysis of the radius of curvature of the convex and concave sides. An average of 5 points (range, 4-9) was marked along the convex and concave sides of the vertebral body of the experimental and control vertebrae and a computer program was used to fit a circle through the

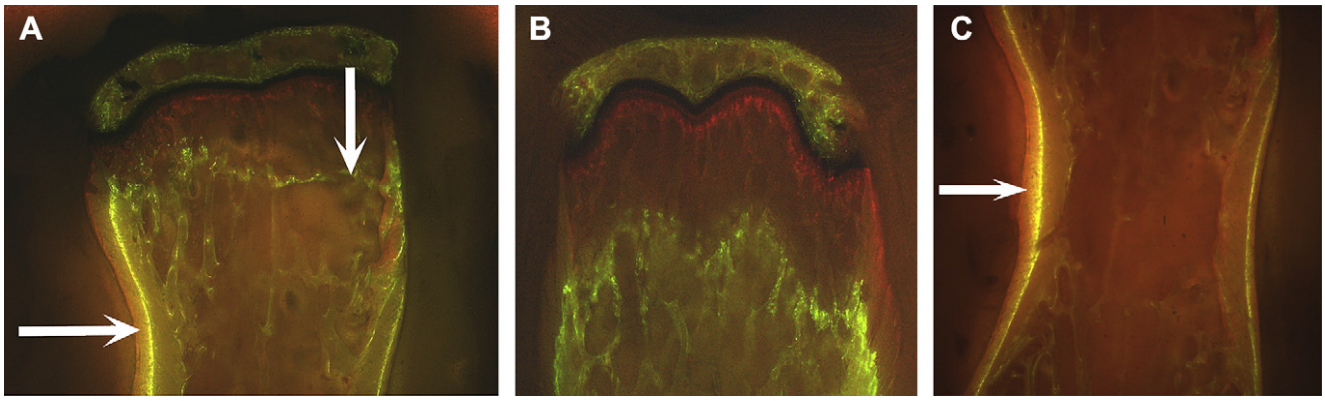

Fig. 5. Photomicrograph of the proximal part of the experimental vertebra from a group 1 animal with calcein (green) and xylenol (orange) staining. The calcein labeling shows increased growth on the convex side (vertical arrow) compared with the concave side. There is considerable increased new bone formation on the concave side (horizontal arrow) (A). Photomicrograph of the proximal part of the control vertebra showing symmetric growth (B). Photomicrograph of the mid-vertebral body of the experimental vertebra showing increased new bone formation on the concave side with vertebral body remodeling (horizontal arrow) (C).

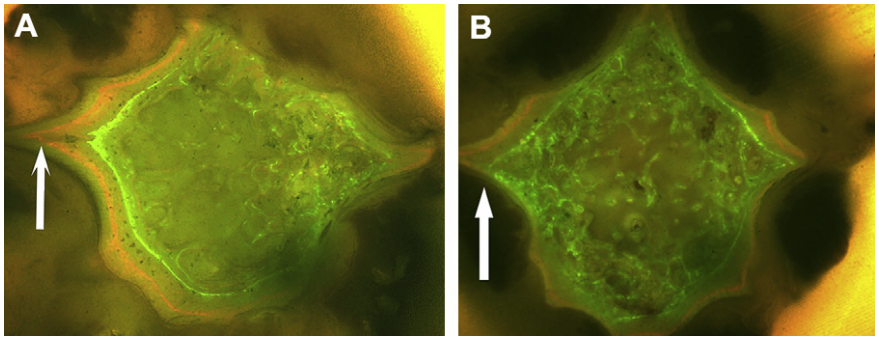

Fig. 6. Photomicrograph of an axial (transverse) section through the mid-vertebral body of the experimental vertebra with calcein (green) and xylenol (orange) staining. There is new bone formation on the concave side (vertical arrow) and a drift of the vertebral body towards the convex side (A). Photomicrograph of an axial section through the mid-vertebral body of the control vertebra showing symmetric new bone formation (vertical arrow) without any vertebral body drifting (B).

points. The radius of curvatures of circles fitted to the convex and concave sides of the vertebrae at weeks 1 and 6 estimated the amount of ''bending'' of the vertebral body.

Undecalcified vertebrae sections imaged with fluorescent microscopy were evaluated by marking an average of 20 (range, 5-38) points along the end of the vertebra, along the growth plate, and along the calcein-labeled ossification front of the metaphyseal bone (Fig. 1). A computer program using linear regression then fit a straight line through each set of points. The angulation between the lines on either side of the epiphysis measured the epiphyseal wedging and the angulation between the xylenol-labeled physis and the calcein-labeled ossification front measured asymmetric growth (Fig. 1 and Fig. 5A). The width of the cortex on the convex and concave side of the experimental and control vertebrae in the mid-vertebral body was measured from micrographs of the decalcified (H&E stained) sections (Fig. 5C).

The epiphyseal wedging and asymmetrical growth measurements were extrapolated linearly to a value for the 6-week experiment (groups 1-3) by multiplying the measured angle by a factor of 1.2 (ratio between the 6-week experiment and 5-week time between fluorescent markers).

The amount of vertebral wedging that was caused by vertebral body remodeling was inferred by subtracting the amount of wedging caused by epiphyseal wedging and asymmetrical growth from the total vertebral wedging. The cortical thickness asymmetry was measured from the experimental and control vertebrae as the mid-vertebral body cortical thickness of the convex side in microns subtracted from that of the concave side.

Statistical analysis

Analyses were performed with SPSS (version 12.0.1, SPSS Inc, Chicago, IL). Group-wise comparative single variable *t* tests were used to determine whether the measures of asymmetrical shape of the vertebrae were significantly different from zero, and paired *t* tests were used in each group of animals to identify differences between experimental and control vertebrae. The differences in total wedging, asymmetrical growth, epiphyseal wedging, inferred vertebral body wedging, vertebral body bending, and cortical thickness were compared between the groups of animals vertebrae using one-way ANOVA with post-hoc (Bonferroni correction) between-group multiple comparisons. A p-value less than .05 was considered statistically significant.

Results

The average growth of the experimental vertebrae as a percentage of that of the control vertebrae was 56% in group 1, 39% in group 2, 25% in group 3, and negligible in group 4 (growth measured from 1-week and 6-week CT

Table 1
Total amount of vertebral wedging ± standard deviation (experimental and control vertebrae), the epiphyseal wedging, metaphyseal wedging (asymmetrical growth), vertebral body apparent bending for each group (experimental vertebrae). A positive sign indicates wedging towards the concavity, and a negative sign indicates wedging towards the convexity. Total wedging was measured from micro-CT Images; epiphyseal and metaphyseal wedging were measured from fluorochrome labels.

Group (Age / Loading)	Control vertebral wedging (total) (degrees)	Experimental wedging (total) (degrees)	Epiphyseal wedging (degrees)	Metaphyseal wedging (asymmetrical growth) (degrees)	Vertebral body wedging (inferred) (degrees)
Group 1 (5-week old / 0.1 MPa)	3±4	18±12	9±8	8±10	1±11
Group 2 (14-week old / 0.1 MPa)	0±4	6±6	0±12	1±2	5±16
Group 3 (14-week old / 0.2 MPa)	1±3	10±6	3±7	4±3	3±5
Group 4 (32-week old / 0.2 MPa)	1±1	5±6	−1±4	0±1	7±6

Table 2
Vertebral body apparent bending for each group (based on differences in the curvature of the convex and concave sides).

	Vertebral body apparent bending (degrees)	
	Experimental	Control
Group 1	18±25	4±3
Group 2	−1±12	0±6
Group 3	7±10	4±11
Group 4	3±7	5±10

images). The growth rates of the control vertebrae in the 14- and 32-week old animals were 16% and 3% that of the 5-week old animals, respectively.

All animals developed vertebral wedging during the 6-week study (Figs. 4A and 4B). The wedging of the experimental vertebra compared with the control vertebra was statistically significant in groups 1, 2 and 3. The total vertebral wedging of the experimental vertebrae that developed during the 6-week study decreased with increasing animal age and increased with increased loading: 18° in group 1, 6° in group 2, 10° in group 3, and 5° in group 4 (Table 1). In comparisons between groups by analysis of variance, both the total wedging of experimental vertebrae and the amount of asymmetric growth was greater in group 1 than in groups 2 and 4 ($p < .05$).

The contribution of asymmetric growth to the total vertebral wedging was 44% in group 1 (Fig. 5A) and 17% and 40% respectively in groups 2 and 3 (Table 1). Asymmetric growth and epiphyseal wedging were significant in group 1 ($p < .05$), and asymmetric growth was significant in group 3 ($p < .01$). The inferred vertebral body contribution to the total wedging of the experimental vertebrae averaged 1°, 5°, 3°, and 7° in groups 1 through 4 respectively (Table 1), and this was statistically significant in group 4 ($p < .05$).

The micro CT images showed that the experimental vertebrae were not only becoming wedged, but that the vertebral bodies were also becoming deformed. The initially biconcave vertebrae gradually developed increased curvature on the concave side of the curve and decreased curvature on the convex side. This suggested that the vertebrae were either bending, or that the cortices were remodeling selectively at their internal and external surfaces (Figs. 4A and 4B).

In addition, cortical thickness measurements indicated more new bone formation on the concave side than on the convex side of the vertebrae (Figs. 4B, 5C, 6A and 6B) (Table 3). The contribution of the vertebral body remodeling to the total wedging was estimated as 6%, 83%, 30%, and 140% in groups 1 through 4 respectively (Table 1). The vertebral body apparent bending, estimated from the radii of curvature measured from micro CT images (Table 2), was compared with the vertebral body wedging inferred by subtracting metaphyseal and epiphyseal wedging from total wedging (Table 1). This comparison indicated that apparent bending was greater than the inferred vertebral body wedging in groups 1 and 3, was negligible in group 2, and was 50% of the inferred wedging in group 4. In groups 1, 2 and 4, the cortical thickness measured from coronal plane histological sections was greater on the concave side compared with the convex side (Fig. 5C), and this difference was significant ($p < .05$) in group 1 (Table 3). Together, these observations indicate substantial remodeling of the cortices, with thickening on the concave side of the imposed curve and resorption and apposition effectively ‘‘translating’’ the mid-vertebral body towards the convexity of the imposed curve.

Discussion

This study demonstrated that caudal vertebrae, when loaded with asymmetric compression forces, developed wedging that was caused by a combination of asymmetrical growth, vertebral body remodeling, and epiphyseal wedging. Circumferential growth of the epiphysis is minimal so the epiphyseal wedging is considered remodeling, not growth. The relative contributions to vertebral wedging varied between groups of animals; asymmetric growth was most important in younger animals and vertebral remodeling was most important in older animals. In groups 2 and 3, the deformity was greater with the higher stressed (group 3) vertebrae. The vertebral wedging was distributed differently between its component parts (asymmetric growth, epiphyseal wedging, and vertebral body remodeling) and this distribution differed in the 4 groups (Table 1). In group 1, total wedging was almost equally distributed between the epiphysis and asymmetric growth. In groups 2 and 3, the total wedging was greater in group 3 (0.2 MPa) and was almost equally divided between the 3 components, whereas the greatest contribution was vertebral body remodeling (77%) in group 2. In group 4, the total wedging resulted entirely from vertebral body remodeling.

Table 3
Mid-vertebral body cortical thickness (microns) measured from the two sides of coronal plane sections of experimental and control vertebrae.

	Experimental			Control			
	Concave	Concave	Difference (concave - convex)	Concave	Concave	Difference (concave - convex)	Mean of right and left sides
Group 1	855±473	487±105	369±535	565±139	645±153	−80±77	605±535
Group 2	758±118	790±157	−33±84	758±205	823±365	−73±240	795±271 (n=3)
Group 3	661±142	529±81	131±188	609±238	606±261	3.8±141	607±239
Group 4	860±478	669±239	191±285	623±478	777±105	−153±197	700±116

The rat model used in this study has several limitations. The tail vertebrae do not have any posterior elements and this study only addressed the 2-dimensional deformity in the coronal plane (scoliosis); we did not evaluate deformities in the sagittal plane (kyphosis) or axial plane (vertebral rotation). However, because the tail vertebrae of rats are almost cylindrical, we believe that this model allows inferences relative to sagittal plane curvature also. The tail vertebrae are normally physiologically loaded only as a result of muscle forces. The vertebrae develop ossified epiphyses whereas humans do not develop a secondary ossification center. However, rats grow fast, reaching skeletal maturity at an early age, permitting the 6-week duration of the experiment. Rat caudal vertebrae are relatively longer and narrower than human vertebrae. It is possible that rat cortical and cancellous bone may respond differently to asymmetric loading.

There is considerable variability in the results for vertebral wedging, with 3 likely sources of this variability. These were 1) positioning variability in the CT and selection of the image plane; 2) operator error (choosing different points for the angle measurements); and 3) the variability between animals in each group. Each CT image was examined to identify the likely sources of any measurements error, and it appeared that actual variability between animals in each group was the major source of variability. This in turn probably resulted from the construct design in this study where the instrumentation spanned 2 discs as well as the vertebra. This often caused an asymmetrical deformity with more disc wedging at one end of the construct than the other end.

The vertebral body remodeling may have been a result of both cortical remodeling (apposition and/or resorption) and cortical lengthening and shortening, producing bending of the vertebral body. In group 1, there was a substantial amount of asymmetry between the curvatures of the convex versus concave sides, but this contributed little to the overall vertebral wedging, suggesting that apposition/resorption predominated.

In a study using a bent tail without superimposed compression, Pazzaglia et al. did not find any remodeling in their adult animals [16], whereas our study showed remodeling in older animals similar to remodeling in the younger animals, although of less magnitude. These differences may be explained by the superimposed compressive loading in the present study. A similar study involving only young animals concluded that asymmetrical growth was the sole cause of the vertebral wedging [7]. The present study, which included older animals, documented that vertebral body wedging was caused by a combination of epiphyseal wedging, asymmetric growth, and vertebral body remodeling with asymmetric growth becoming less important in older animals.

The mechanism producing wedging of the vertebral body is unclear, and may involve relative length changes of the concave sides, bending and cortical remodeling by apposition and/or resorption (Fig. 1). Similarly, diaphyseal realignment of the tibia after experimental fractures was documented in an immature rat tibia model by Li et al., who created a mid-shaft tibial fracture and fixed it with an intramedullary pin imposing 27° more than normal anterior tibial bow [12]. During the 12-week experiment, the angulation corrected from 27° to 10.5°. The correction measured at the proximal tibial growth plate was 8°, indicating that the majority of correction was caused by diaphyseal remodeling, identified as ‘‘cortical drift.’’

The findings from the mature and adult animals may have important implications for patients with AIS who are past their peak growth velocity, suggesting that in older patients an appropriate amount of asymmetrical loading applied for a sufficient amount of time may correct scoliosis and vertebral wedging with minimally invasive nonfusion surgical techniques. A study with nitinol shape-memory alloy intramedullary rods used to create a diaphyseal deformity in the rabbit tibia showed that rods with a smaller radius of curvature generated enough force to create a deformity with diaphyseal remodeling (Wolff’s law) [17].

The findings in the present study may also have important implications for the etiology of kyphosis in older patients. Kyphosis in the elderly has been attributed to compression fractures, but in many people the deformity has an insidious onset without any history of pain and a distinct fracture is often not seen on standard Radiographs. A study of human cadaver specimens tested the hypothesis that kyphotic deformities in the elderly may develop from a gradual time-dependent ‘‘creep’’ process, rather than a fracture [18]. It appears that in addition to growth modulation at the growth plate, the contribution of vertebral body remodeling to progressive vertebral deformities in both skeletally immature and mature patients should be taken into account.

Acknowledgment

The authors thank the Scoliosis Research Society for supporting this study and Bob Trautwine, Stryker Surgical, Burlington, Vermont Area for providing the oscillating drill used to place percutaneous pins.

References

[1] Lonstein JE, Carlson JM. The prediction of curve progression in untreated idiopathic scoliosis during growth. *J Bone Joint Surg Am* 1984;66-A:1061–71.

[2] Mente PL, Stokes IA, Spence H, et al. Progression of vertebral wedging in an asymmetrically loaded rat tail model. *Spine (Phila Pa 1976)* 1997;22:1292–6.

[3] Bylski-Austrow DI, Wall EJ, Glos DL, et al. Spinal hemiepiphysiodesis decreases the size of vertebral growth plate hypertrophic zone and cells. *J Bone Joint Surg Am* 2009;91-A:584–93.

[4] Stokes IA, Spence H, Aronsson DD, et al. Mechanical modulation of vertebral body growth. Implications for scoliosis progression. *Spine (Phila Pa 1976)* 1996;21:1162–7.

[5] Roaf R. Vertebral growth and its mechanical control. *J Bone Joint Surg Br* 1960;42-B:40−59.

[6] Braun JT, Hoffman M, Akyuz E, et al. Mechanical modulation of vertebral growth in the fusionless treatment of progressive scoliosis in an experimental model. *Spine (Phila Pa 1976)* 2006;31:1314−20.

[7] Mente PL, Aronsson DD, Stokes IA, et al. Mechanical modulation of growth for the correction of vertebral wedge deformities. *J Orthop Res* 1999;17:518−24.

[8] Betz RR, D'Andrea LP, Mulcahey MJ, et al. Vertebral body stapling procedure for the treatment of scoliosis in the growing child. *Clin Orthop Relat Res* 2005;434:55−60.

[9] Aronsson DD, Stokes IA. Nonfusion treatment of adolescent idiopathic scoliosis by growth modulation and remodeling. *J Pediatr Orthop* 2011;31:S99−106.

[10] Rubin CT, Lanyon LE. Kappa Delta Award paper. Osteoregulatory nature of mechanical stimuli: function as a determinant for adaptive remodeling in bone. *J Orthop Res* 1987;5:300−10.

[11] Schulte FA, Lambers FM, Kuhn G, et al. In vivo micro-computed tomography allows direct three-dimensional quantification of both bone formation and bone resorption parameters using time-lapsed imaging. *Bone* 2011;48:433−42.

[12] Li J, Ahmed M, Samnegard E, et al. Spontaneous correction of angular fracture deformity in the rat. *Acta Orthop* 2005;76:434−41.

[13] MacLean JJ, Lee CR, Grad S, et al. Effects of immobilization and dynamic compression on intervertebral disc cell gene expression in vivo. *Spine (Phila Pa 1976)* 2003;28:973−81.

[14] Aronsson DD, Stokes IA, McBride C. The role of remodeling and asymmetric growth in vertebral wedging. *Stud Health Technol Inform* 2010;158:11−5.

[15] Stokes IA, Aronsson DD, Dimock AN, et al. Endochondral growth in growth plates of three species at two anatomical locations modulated by mechanical compression and tension. *J Orthop Res* 2006;24:1327−34.

[16] Pazzaglia UE, Andrini L, Di Nucci A. The effects of mechanical forces on bones and joints. Experimental study on the rat tail. *J Bone Joint Surg Br* 1997;79-B:1024−30.

[17] Firoozbakhsh K, Moneim MS, Yi IS, et al. Smart intramedullary rod for correction of pediatric bone deformity: a preliminary study. *Clin Orthop Relat Res* 2004;424:194−201.

[18] Pollintine P, Luo J, Offa-Jones B, et al. Bone creep can cause progressive vertebral deformity. *Bone* 2009;45:466−72.